electronics

MDPI

Article

Evaluating Photovoltaic Conversion Performance under Artificial Indoor Lighting

Cecilia Guillén

Centro de Investigaciones Energéticas Medioambientales y Tecnológicas (CIEMAT), Avda. Complutense 40, 28040 Madrid, Spain; c.guillen@ciemat.es

Abstract: Several photovoltaic technologies, based on different semiconductor absorbers with band-gap energy in the range E_g = 1.0–1.5 eV are currently sharing the market for outdoor applications. These photovoltaic cells are designed to achieve an optimal photovoltaic conversion under solar illumination (represented by the standard AM1.5 global spectrum), but their performance changes under different artificial indoor lights. Here, the detailed balance principle that was first applied for an ideal photovoltaic absorber under solar radiation is now used by considering the actual spectra of four typical indoor lamps: incandescent, halogen, metal halide and white LED. For each particular illumination source, the theoretical maximum for short-circuit current, open-circuit voltage and maximum power point have been calculated and represented as a function of the absorber band-gap energy. Furthermore, the optical absorption spectra of some semiconductors with optimal solar conversion efficiencies are used to estimate their comparative performance under the various artificial light sources. It has been found that wide band-gap absorbers (E_g~1.9 eV) are needed to achieve a light-to-electricity conversion efficiency of 60% under LED illumination or 31% with metal halide bulbs, while a lowest band-gap energy of about 0.8 eV is required to obtain a maximum efficiency of 24% with incandescent and halogen lamps.

Keywords: photovoltaic cells; artificial lights; efficiency limit calculation; energy harvesting

Citation: Guillén, C. Evaluating Photovoltaic Conversion Performance under Artificial Indoor Lighting. *Electronics* **2024**, *13*, 3378. https://doi.org/10.3390/electronics13173378

Academic Editor: Fabio Corti

Received: 14 July 2024
Revised: 17 August 2024
Accepted: 24 August 2024
Published: 26 August 2024

1. Introduction

Photovoltaic devices, which directly convert light into electricity, are considered one of the key renewable energy sources. They are usually developed to collect energy from outdoor solar radiation and then characterized under a standard AM 1.5 global spectrum [1], which corresponds to 1000 W/m^2 perpendicular solar radiation on the Earth's surface at air mass 1.5 [2]. This procedure allows comparing different photovoltaic performances, but it does not represent the real conditions either for outdoor or for indoor usage. While for outdoor applications a typical daylight is in the 50–1000 W/m^2 range, indoor devices have to operate below 50 W/m^2 [3]. Despite the low energy flux, indoor applications are receiving great attention because artificial light harvesting by suitable photovoltaic cells can power low-consumption components for the Internet of Things in smart homes and smart cities [4]. For this purpose, the use of supercapacitors allows operation when ambient light is unavailable, prolonging the working time with a low environmental impact [5].

There are several photovoltaic technologies, based on different semiconductor absorbers such as crystalline silicon (c-Si), cadmium telluride (CdTe) and copper indium gallium selenide ($CuIn_{1-x}Ga_xSe_2$ or CIGS), which currently share the market for outdoor applications [6]. CIGS belongs to the I–III–VI_2 semiconductor alloys with a chalcopyrite structure, presenting the advantage of an adjustable band-gap energy from E_g = 1.0 eV ($CuInSe_2$) to 1.7 eV ($CuGaSe_2$) for selenide compounds [7], or from E_g = 1.5 eV ($CuInS_2$) to 2.4 eV ($CuGaS_2$) considering sulfides [8]. The toxicity of Cd and the low elemental abundance of In and Ga have motivated the investigation of alternative photovoltaic absorbers in I_2–II–IV–VI_4 compounds, which are isoelectronic equivalent of the I–III–VI_2

semiconductors. In fact, copper zinc tin sulfo-selenide ($Cu_2ZnSnS_{2-x}Se_x$ or CZTS) has already demonstrated good solar conversion efficiency [9], with a band-gap ranging from 1.0 eV ($Cu_2ZnSnSe_4$) to 1.5 eV (Cu_2ZnSnS_4), and the possibility of increasing to 2.3 eV (Cu_2ZnGeS_4) by Ge-alloying [10]. Taking into account that only photons with energies above the band-gap are absorbed, the photogenerated current tends to increase, while the photovoltage decreases as the absorber E_g decreases [11]. Then, the photovoltaic power will reach a maximum at certain E_g values. Notwithstanding the above, novel organic compounds and nanostructured materials, as well as multi-junction devices, are being developed to better exploit the solar spectrum by adding more than one absorption edge [1]. In particular, the flexible optical characteristics of perovskite materials that combine organic and inorganic cations with halide anions make them good candidates for both outdoor and indoor applications [1,4].

The maximum light to electricity conversion efficiency (η) of a single junction photovoltaic cell was first calculated approximating the sun spectrum by the emission of a black body with a surface temperature of 6000 K [12], and later by using the standard AM1.5 global spectrum [13]. These calculations give an optimal range for photovoltaic conversion under solar illumination at E_g = 1.0–1.5 eV, according to the experimental results obtained with different absorber materials [14]. However, if the same question is asked for indoor applications, there is no single answer because the optimal band-gap energy will depend on the specific illumination source. Several researchers have already measured the photovoltaic conversion of radiation emitted by different artificial lights, such as halogen, fluorescent or other gas-discharge lamps [15], and recently white light LEDs [16]. Most of the research is focused on commercially available devices [4,17], although alternative materials are also being investigated [18,19].

In this work, the detailed balance principle that was first applied for an ideal photovoltaic absorber under solar radiation by Shockley and Queisser [12] is now used for different artificial light sources, taking into consideration the real spectra of four typical indoor lamps: incandescent, halogen, metal halide and white LED. For each particular illumination source, the determination of the efficiency limit includes the calculation of the theoretical maximum for the various characteristic photovoltaic parameters (short-circuit current, open-circuit voltage and maximum power point), which are represented as a function of the absorber band-gap energy. In parallel, the optical absorption spectra of some semiconductors with the best efficiencies under solar radiation are compared, and their performance under the different artificial light sources is estimated. This information is useful to select which of the commercial solar cells is most suitable for each indoor illumination, while also indicating their output current and voltage characteristics to power small electronic devices.

2. Photovoltaic Absorbers and Light Sources

The best photovoltaic conversion efficiencies confirmed under standard solar radiation are reported by Green et al. [20] and some illustrative data are included in Table 1. The highest value corresponds to cells based on c-Si absorber, closely followed by cells based on different chalcogenide compounds (CdTe, CIGS and CZTS), which have been mentioned in the previous section. The photovoltaic performance is determined mainly by the intrinsic material properties (complex refractive index n + ik) and its thickness t, being the absorption coefficient $\alpha = 4\pi k/\lambda$ and the optical absorptance $A(\lambda) = 1 - e^{-\alpha(\lambda)t}$ [21], expressed as a function of the radiation wavelength λ. Figure 1 compares the absorptance spectra obtained for the selected semiconductors, taking the respective extinction coefficient data, k(λ), from the refractive index database [22]. It should be noted that different thicknesses are used to achieve 100% absorptance at $E \geq E_g$. While for c-Si the required thickness is about 0.3 mm [23], lower values around 3 μm are needed for CdTe [24] or 2 μm for both CIGS [25] and CZTS [9]. These chalcogenide compounds are commonly prepared by thin-film deposition on glass substrates, but c-Si wafers are mechanically cut from

crystalline-grown ingots. In all cases, a front glass is used to protect the photovoltaic cell, which has a significant absorptance at $\lambda < 350$ nm, as shown in Figure 1.

Table 1. Confirmed efficiencies for single-junction cells measured under the global AM1.5 spectrum (1000 W/m^2) at 25 °C [20].

Photovoltaic Cell Acronym	Absorber Semiconductor	Absorber E_g (eV)	Solar Conversion Efficiency (%)
c-Si	Crystalline Si	1.12	26.7 ± 0.5
CdTe	CdTe	1.45	22.3 ± 0.2
CIGS	$CuIn_{1-x}Ga_xSe_2$	1.30	23.6 ± 0.4
CZTS	$CuZnSnS_{2-x}Se_x$	1.03	14.9 ± 0.3

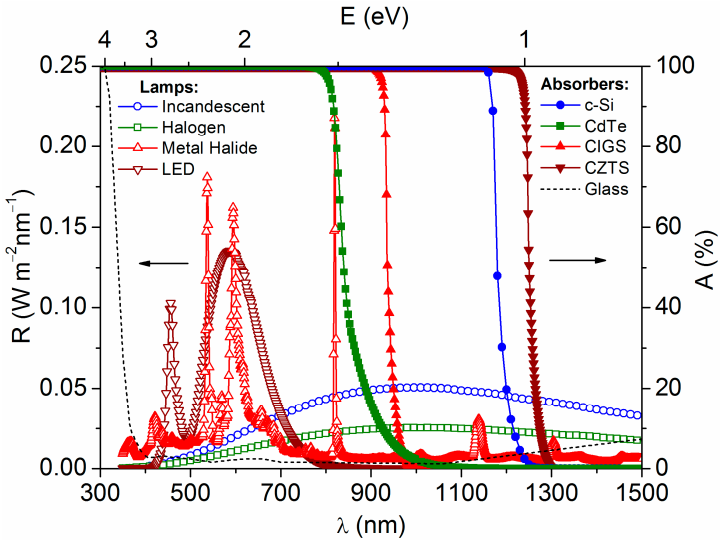

Figure 1. Spectral radiance of typical artificial light sources and optical absorptance corresponding to different photovoltaic absorbers and the front glass. Data are shown as a function of wavelength (λ) and energy ($E = hc/\lambda$).

In order to evaluate the photovoltaic performance under typical indoor conditions, several commercial light sources have been considered in this work. They were selected to illustrate different spectral radiances, which were obtained from the National Oceanic and Atmospheric Administration (NOAA) database [26] as depicted in Figure 1. Although the representation of the radiance (R) versus λ is the most used, the figure shows also the dependence on light energy ($E = hc/\lambda$) to better illustrate the subsequent calculations that are carried out in terms of energies. The various artificial light sources can be grouped into three categories. One of them is constituted by incandescent and halogen lamps, with smooth spectra corresponding to a blackbody radiator at 2800 K, giving a maximum radiance around $\lambda = 950$ nm [27]. Another group includes fluorescent bulbs, high-pressure sodium and metal halide lamps, with multiple emission peaks and correlated color temperatures between 2000 K and 6000 K depending on the composition of the internal gas [28]. The last group is made up of LED lamps, which have two emission peaks centered at λ_1~450 nm and λ_2~600 nm, increasing their color temperature with the ratio between both maxima (I_1/I_2) as reported by [29]. The various light sources represented in Figure 1 have a similar correlated color temperature (near 2800 K) and different illumination densities. Artificial light spectra are shown unnormalized and the respective total light intensities are calculated by integrating each spectrum over the same region as standard sunlight. They range from 58 W/m^2 for the incandescent lamp to 30 W/m^2 for the halogen source and 22 W/m^2 for the metal halide and LED lamps. These intensities are common in the lighting of commercial and work buildings, although the increasing improvement of LED systems is allowing values around 3 W/m^2 to be used in some office environments.

3. Photovoltaic Performance Analysis

3.1. Photogenerated Current Density and Recombination Losses

Figure 2 illustrates the main input and output parameters that are considered here to evaluate the photovoltaic performance according to the ideal model developed by Shockley and Queisser [12]. For the balanced photovoltaic converter, at zero output voltage, all electron–hole pairs generated by the incident radiation can in principle be extracted as current into the external circuit, giving a maximum current density (J_{max}) that depends on the incident photon flux (F_i) and the material absorptance. The incident photon flux is calculated for each lamp represented in Figure 1, from the respective spectral radiance:

$$F_i = \frac{q\lambda}{hc}R(\lambda) = \frac{q}{E}R(E), \tag{1}$$

where q is the elementary charge, h is the Planck constant, c is the vacuum speed of light, and E is the photon energy related to the respective wavelength. Then, the maximum current density is given by the integration of the incident photon flux with the material absorptance, considering $A(E < E_g) = 0$ and $A(E \geq E_g) = 1$ for each photovoltaic absorber with band-gap energy E_g [13]:

$$J_{max}(E_g) = \int_{E=0}^{E=\infty} A(E)F_i(E)dE = \int_{E=E_g}^{E=\infty} F_i(E)dE. \tag{2}$$

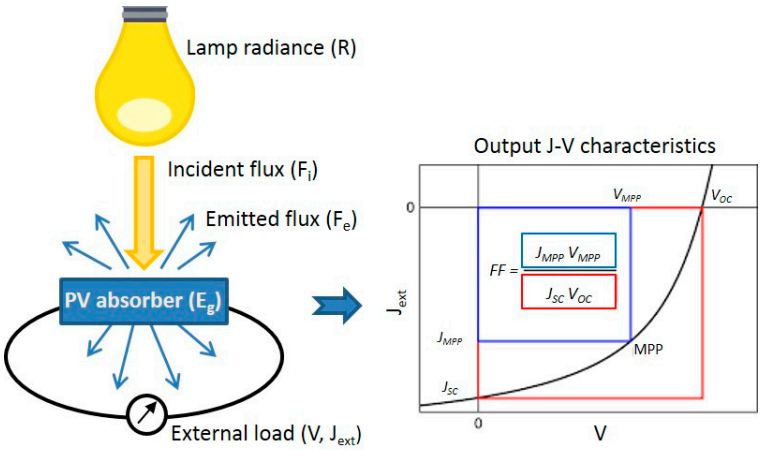

Figure 2. Operating diagram of a photovoltaic cell with front illumination. The cell at voltage V emits photons from its top and bottom according to [12]. The output parameters are explained throughout the text.

At non-zero output voltage, the concentration of electron–hole pairs inside the semiconductor material exceeds the equilibrium concentration and some of the energy stored in the photo-generated electrons and holes and internal luminescence are lost through different recombination processes and emission of luminescent photons. Non-radiative recombination mediated by defects and impurities can be neglected in the ideal limit, but there are radiative losses that are independent of the material quality and give an emitted photon flux according to the generalized Planck law [30]:

$$F_e(E,V) = \frac{2\pi E^2}{h^3c^2\left[\exp\left(\frac{E-qV}{kT_c}\right)-1\right]} \tag{3}$$

where V is the external applied voltage, k is the Boltzmann constant and T_c is the photovoltaic cell temperature, which is assumed 300 K in the model [12]. Subsequently, the radiative recombination current density can be calculated as:

$$J_{rad}(E_g, V) = 2q\int_{E=0}^{E=\infty} A(E)F_e(E, V)dE = 2q\int_{E=E_g}^{E=\infty} F_e(E, V)dE, \quad (4)$$

where the factor 2 is due to the assumption that the photovoltaic converter emits radiation from the front and rear sides, as illustrated in Figure 2.

Both J_{max} and J_{rad} are calculated by entering Equations (2) and (4) into OriginPro 8 software (a widely used commercial program) and they are represented in Figure 3 for the different artificial light sources as a function of the absorber band-gap energy. For the incandescent and halogen lamps, the evolution of J_{max} with E_g is analogous to that reported under solar radiation [13], with a fast decrease when the energy increases from 0.5 to 2.0 eV. For typical c-Si solar cells with E_g = 1.1 eV, the obtained values are J_{max} = 19 A/m^2 under the incandescent light (58 W/m^2) and J_{max} = 10 A/m^2 under the halogen lamp (30 W/m^2), which are consistent with J_{max} = 440 A/m^2 reported under standard sunlight (1000 W/m^2) [13], taking into account the respective illumination intensity. A smoother decay is observed for the metal halide lamp and a plateau for the LED at energies lower than 1.8 eV. This is because LED radiation is located in a short wavelength range (400–700 nm) that can be absorbed by any semiconductor with $E_g \leq 1.8$ eV, but for the other lights the radiance extends to longer wavelengths, where it can only be absorbed by lower E_g values (Figure 1).

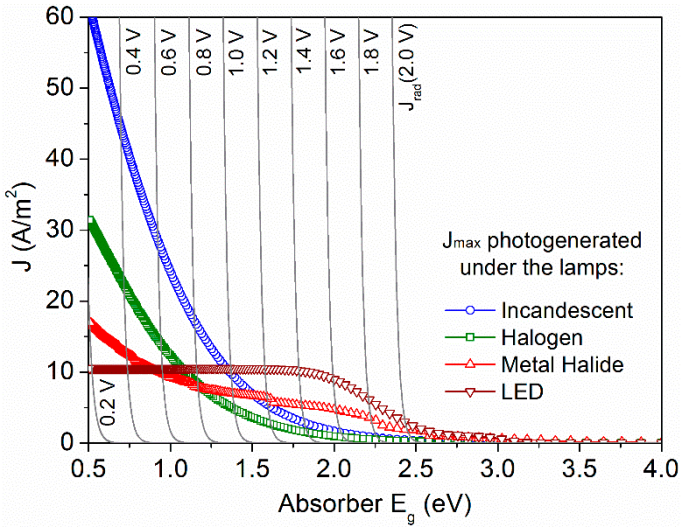

Figure 3. Maximum current density J_{max} (at V = 0) and radiative recombination current density J_{rad} (at $V \neq 0$) calculated for the different lamps as a function of the absorber band-gap energy.

The external current density is the sum of all the current densities in the cell:

$$J_{ext}(E_g, V) = J_{max}(E_g) - J_{rad}(E_g, V), \quad (5)$$

giving an equation that describes the output current-voltage characteristics of each photovoltaic cell. These are also defined by the cell parameters called short-circuit current density (J_{SC}), open-circuit voltage (V_{OC}) and fill factor (FF), as depicted in Figure 2.

The short-circuit current density corresponds to the generation of electron–hole pairs by incident light from which the thermal recombination at zero bias has to be subtracted:

$$J_{SC}(E_g) = J_{max}(E_g) - J_{rad}(E_g, V = 0). \quad (6)$$

According to Figure 3, the value of J_{rad} at V = 0 is zero in the range of interest (that is for $E_g \geq 0.5$ eV), where the short-circuit current is equal to the maximum photogenerated current ($J_{SC} = J_{max}$).

On the other hand, the maximum output voltage occurs in the open-circuit condition (V_{OC}), when the current extracted by the external circuit is zero:

$$J_{rad}(E_g, V_{OC}) = J_{max}(E_g) \;\Rightarrow\; 2q\int_{E=E_g}^{E=\infty} F_e(E, V_{OC})dE = \int_{E=E_g}^{E=\infty} F_i(E)dE\,. \tag{7}$$

Since the function F_i (incident photon flux given by the lamp radiance) has no analytical expression, Equation (7) has no analytical solution. Therefore, the V_{OC} values shown in Figure 4 are obtained numerically from the J_{rad} and J_{max} data represented in Figure 3. It should be noted that higher open-circuit voltages may be gained if the temperature of the photovoltaic cell is reduced towards zero. Under these circumstances, the emitted photon flux tends to zero and the V_{OC} tends to the band-gap potential E_g/q [12]. However, at room temperature (T_c = 300 K) the open-circuit voltage has a lower value that is represented in Figure 4 for the different light radiances. The range of interest is considered to end at E_g = 2.5 eV, because according to Figure 3 no significant photocurrent can be generated with higher band-gap energies. In the analyzed region ($0.5 \leq E_g \leq 2.5$ eV), the open-circuit potential follows a linear dependence in the form $V_{OC} = a + bE_g/q$, as reported under solar illumination [13]. The data in Figure 4 evidence that the independent term decreases, from $a = -0.22$ to $a = -0.30$, when the overall light power decreases, from $P_i = 58$ W/m^2 for the incandescent bulb to $P_i = 22$ W/m^2 for the metal halide and LED lamps. Such a decrease of V_{oc} with the illumination power is expected [3,31], but it is only seen at band-gap energies below 1.5 eV. The behavior changes because at $E_g \geq 1.5$ eV the photogenerated current is greater for the metal halide and LED lamps (Figure 3), and this increases the corresponding slope value (up to b = 0.95) in comparison with that obtained for the incandescent and halogen lamps (b = 0.89). Consequently, at $E_g \geq 1.5$ eV the open-circuit voltage is higher for the LED than for the incandescent lamp, despite the lower LED power density, approaching that reported by [13] for the standard of 1000 W/m^2 sunlight (which is V_{OC} = 2.15 V for E_g = 2.5 eV).

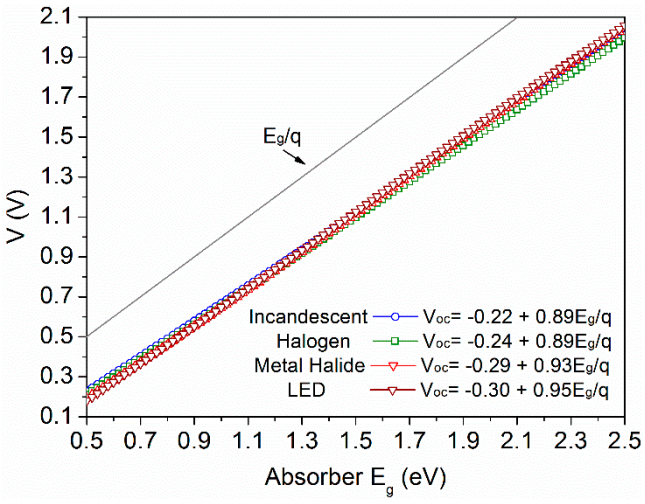

Figure 4. Open-circuit voltage V_{OC} calculated for the different lamps as a function of the absorber band-gap energy.

3.2. Maximum Power Point and Photovoltaic Conversion Efficiency

The maximum power point (MPP) represents the bias potential at which the photovoltaic cell provides the maximum net power, such that $P_{MPP} = J_{MPP}V_{MPP}$ is the maximum of the output J-V curve under illumination (Figure 2). In practice, these values correspond to a particular load resistance that is equal to V_{MPP}/I_{MPP} [17]. Alternatively, in order to

obtain this point from the ideal photovoltaic cell model, the product $V \times J_{ext}$ is calculated for the different lamps and represented in Figure 5 as a function of the absorber band-gap energy. These curves give:

$$V_{MPP}(E_g) = \max[V \times J_{ext}(E_g, V)], \quad (8)$$

$$J_{MPP}(E_g) = J_{ext}(E_g, V_{MPP}). \quad (9)$$

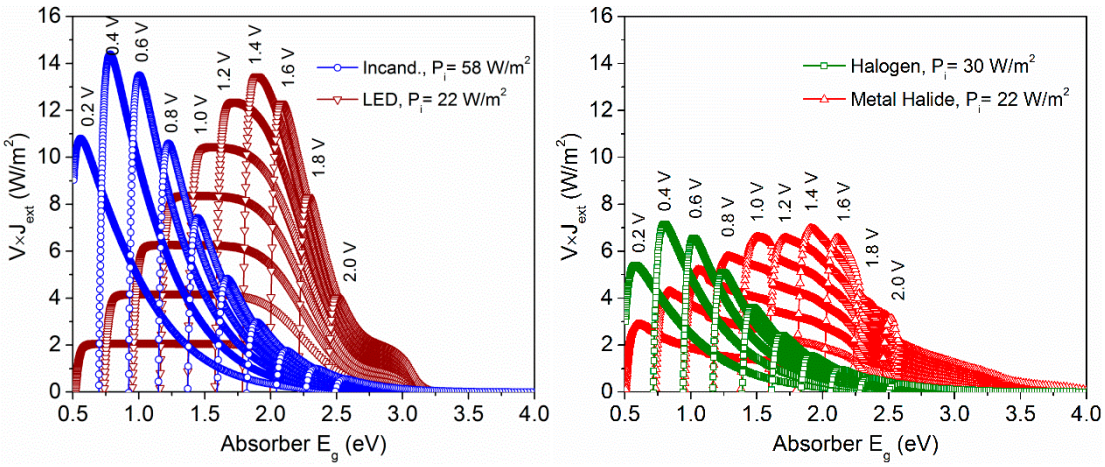

Figure 5. Output power ($V \times J_{ext}$) calculated for the lamps with various illumination densities (P_i) as a function of the absorber band-gap energy, taking the respective data shown in Figure 3.

According to Figure 5, the maximum output power reaches a similar value of around 14 $W/m^{2,}$ for the incandescent and LED lamps, while it is around 7 W/m^2 for the halogen and metal halide lamps. Taking into account the different lighting power density of each source (P_i in the figure), the maximum light to electric power conversion efficiency (η) can be calculated as:

$$\eta = J_{MPP}V_{MPP}/P_i. \quad (10)$$

Moreover, the fill factor (FF) is defined as the ratio of the maximum power to the product of J_{SC} and V_{OC}. This factor indicates the quadrature of the output J-V curves and can be described geometrically by the ratio of two rectangles (as depicted in Figure 2):

$$FF = (J_{MPP}V_{MPP})/(J_{SC}V_{OC}). \quad (11)$$

These parameters (η and FF) are the most significant to determine the photovoltaic quality, and they are represented in Figure 6 for the different artificial lights as a function of the absorber band-gap energy. When illumination is provided by the incandescent and halogen lamps, the efficiency data are practically the same, reaching their greatest values $\eta_{max} = 0.24 \pm 0.01$ at $E_g = 0.84 \pm 0.10$ eV. This corresponds to $V_{MPP} = 0.4$ V in Figure 5 (J_{MPP} of 35 A/m^2 with incandescent light and 18 A/m^2 with halogen light), resulting in a maximum power point voltage that is half the band-gap potential ($V_{MPP} = 0.5E_g/q$). Otherwise, higher absorber band-gap energies are needed to achieve higher conversion efficiencies with the metal halide lamp ($\eta_{max} = 0.31 \pm 0.01$ at $E_g = 1.80 \pm 0.30$ eV) and LED ($\eta_{max} = 0.60 \pm 0.01$ at $E_g = 1.90 \pm 0.10$ eV), which correspond to the same $V_{MPP} = 1.4$ V but different J_{MPP} of 5.0 A/m^2 and 9.5 A/m^2, respectively. In these other cases, the maximum power point voltage is closer to the band-gap potential ($V_{MPP} \sim 0.8E_g/q$), and then closer to V_{OC}, indicating a better photovoltaic quality that is related to an increase of the fill factor with the absorber band-gap energy. Certainly, high-quality factors FF ≥ 0.85 are obtained in Figure 6 for $E_g \geq 1.10$ eV (achieving for LED a FF = 0.91 at $E_g = 1.90$ eV), but the fill factor drops to 0.80 at $E_g = 0.80$ eV, and even below 0.70 with the incandescent and halogen lamps when $E_g \leq 0.60$ eV. This leads to worse conversion efficiencies at the lowest band-gap energies, as reported under solar illumination [13]. The conversion efficiency is

predicted to achieve a value as high as η = 0.60 for an absorber with E_g = 1.90 eV under the LED light spectrum depicted in Figure 1, with P_i = 22 W/m^2. It is in the same order than the theoretical value η = 0.55 obtained for an equivalent absorber under a LED light with P_i = 3 W/m^2 [32], which indicates that the conversion efficiency is not highly dependent on the LED power density. In relation, it is interesting to note that LED arrays with P_i~200 W/m^2 are also considered for office building lighting [33].

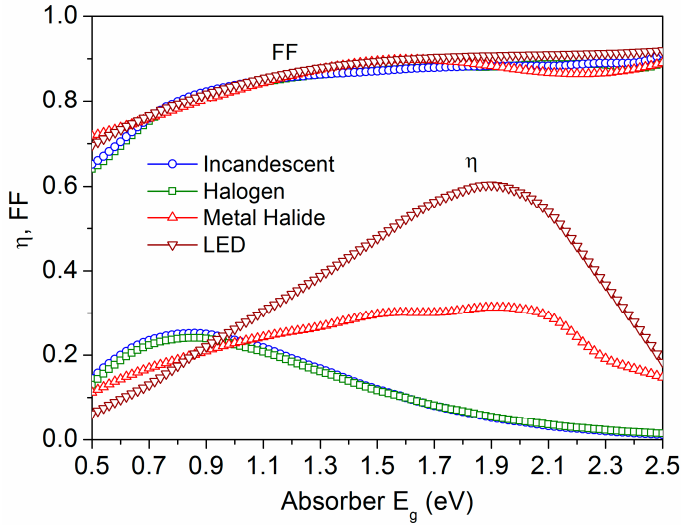

Figure 6. Photovoltaic conversion efficiency (η) and fill factor (FF) calculated for the different lamps as a function of the absorber band-gap energy.

The exploration of new absorber materials has already given record efficiencies greater than 40%, obtained experimentally under LED light with P_i~3 W/m^2 [34], but there are still stability problems and other obstacles that must be resolved for their commercialization [35]. Regarding commercial photovoltaic devices, a solar conversion efficiency η ≥ 0.20 (i.e., 20%) is considered optimal [20], noting that the model gives η = 0.32 ± 0.01 in the range E_g = 1.0–1.5 eV under the standard AM1.5 global spectrum [13]. In Section 2, the characteristics of currently available solar cells with different absorber band-gap energies were presented. Its expected performance under the various artificial light sources analyzed here is illustrated in Figure 7, by applying the results of Figure 6 for the respective E_g value. Both CZTS (E_g = 1.03 eV) and c-Si (E_g = 1.12 eV) show conversion efficiencies in the 20–30% range for the various light sources. The efficiency is also in this range for the other absorbers under metal halide illumination, but under incandescent and halogen lamps it decreases to 15% for CIGS (E_g = 1.30 eV) and below 12% for CdTe (E_g = 1.45 eV). Otherwise, such wider band-gap materials are expected to increase the conversion efficiency to 40–45% under LED illumination. These data are in accord with the results obtained for typical solar cells measured under artificial lights, which confirm the use of c-Si with halogen or incandescent lamps to supply low-power devices [17], and the excellent performance of CdTe under LED illumination [36].

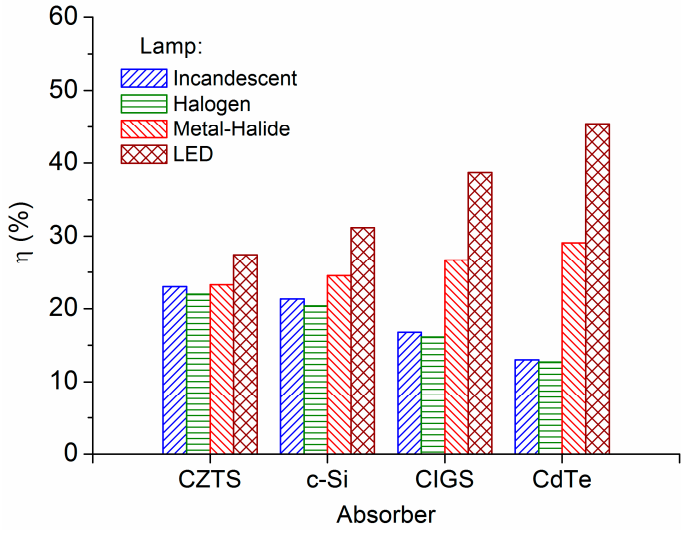

Figure 7. Maximum conversion efficiencies calculated for the different absorber materials and artificial light spectra represented in Figure 1.

4. Conclusions

Applying the detailed balance principle, the photovoltaic performance has been analyzed as a function of the absorber band-gap energy under four different artificial light sources (incandescent, halogen, metal halide and white LED) with a similar correlated color temperature (near 2800 K) and diverse illumination power densities (22–58 W/m^2). The evolution of the maximum photogenerated current (or J_{SC}) is analogous for the incandescent and halogen lamps, with a fast drop when the band-gap energy increases from 0.5 to 2.0 eV. A smoother decay is observed for the metal halide source and a plateau for the LED at $E_g \leq 1.8$ eV, because the LED radiation is located in a small energy range above 1.8 eV while the other lights extend towards lower energies. On the other hand, the open-circuit voltage follows a linear dependence ($V_{OC} = a + bE_g/q$), with an independent term that decreases when the illumination density decreases, but a slope that is greater for the LED lamp despite its lower power, because it provides a higher photogenerated current at $E_g \geq 1.5$ eV.

The maximum conversion efficiency of light into electricity (with respect to the incident illumination power) is of 24% (±1%) at $E_g = 0.84 \pm 0.10$ eV for the incandescent and halogen lamps, increasing to 31% at $E_g = 1.80 \pm 0.30$ eV for the metal halide light and more to 60% at $E_g = 1.90 \pm 0.10$ eV for the LED source. Another indicator of photovoltaic quality is the fill factor, defined as the ratio between the maximum output power and the product of Jsc and Voc, which tends to increase as the band-gap energy increases. Thus, high-quality values FF ≥ 0.85 correspond to $E_g \geq 1.10$ eV (achieving for LED a FF = 0.91 at $E_g = 1.90$ eV), but the fill factor decreases to FF = 0.80 at $E_g = 0.80$ eV, and even below 0.70 for the incandescent and halogen lamps when $E_g \leq 0.60$ eV.

About some commercial photovoltaic devices that are actually developed for outdoor applications, it is estimated that cells based on CZTS ($E_g = 1.03$ eV) and c-Si ($E_g = 1.12$ eV) can offer maximum conversion efficiencies in the 20–30% range for the various artificial light sources. The maximum efficiency is also in this range for wider band-gap absorbers under metal halide illumination, but under incandescent and halogen lamps it decreases to 15% for CIGS ($E_g = 1.30$ eV) and below 12% for CdTe ($E_g = 1.45$ eV). Otherwise, these wider band-gap materials are expected to increase the conversion efficiency to 40–45% under LED lighting.

Funding: This research received no external funding. It is part of a proposal sent to the Spanish Ministry of Science Innovation and Universities (PID2023-148581OB-C33), which as of the date of completion of the manuscript has not been resolved.

Data Availability Statement: The original contributions presented in the study are included in the article; further inquiries can be directed to the corresponding author.

Conflicts of Interest: The author declares no conflicts of interest.

References

1. Oni, A.M.; Mohsin, A.S.M.; Rahman, M.M.; Hossain Bhuian, M.B. A comprehensive evaluation of solar cell technologies, associated loss mechanisms, and efficiency enhancement strategies for photovoltaic cells. *Energy Rep.* **2024**, *11*, 3345–3366. [CrossRef]
2. Xue, Y.; Igari, S. Reference solar spectra and their generation models. *J. Sci. Technol. Light.* **2023**, *46*, 6–18. [CrossRef]
3. Bätzner, D.L.; Romeo, A.; Zogg, H.; Tiwari, A.N. CdTe/CdS solar cell performance under low irradiance. In Proceedings of the 17th European Photovoltaic Solar Energy Conference and Exhibition, Munich, Germany, 22 October 2001; Volume 1, pp. 1180–1183.
4. Bouclé, J.; Ribeiro Dos Santos, D.; Julien-Vergonjanne, A. Doing more with ambient light: Harvesting indoor energy and data using emerging solar cells. *Solar* **2023**, *3*, 161–183. [CrossRef]
5. Wang, C.H.; Huang, K.H.; Wu, C.Y. Enhanced power supply circuitry with long duration and high-efficiency charging for indoor photovoltaic energy harvesting internet of things end device. *IET Power Electron.* **2024**, *17*, 663–674. [CrossRef]
6. Chee, A.K.W. On current technology for light absorber materials used in highly efficient industrial solar cells. *Renew. Sustain. Energy Rev.* **2023**, *173*, 113027. [CrossRef]
7. Rath, C.; Gao, Y.; Koehler, T.; Schmid, M. Impact of band-gap gradient in semi-transparent and bifacial ultra-thin Cu(In,Ga)Se2 solar cells. *Adv. Mater. Interfaces* **2024**, *11*, 2400085. [CrossRef]
8. Barreau, N.; Bertin, E.; Crossay, A.; Durand, O.; Arzel, L.; Harel, S.; Lepetit, T.; Assmann, L.; Gautron, E.; Lincot, D. Investigation of co-evaporated polycrystalline Cu(In,Ga)S2 thin film yielding 16.0% efficiency solar cell. *EPJ Photovolt.* **2022**, *13*, 17. [CrossRef]
9. Zhou, J.; Xu, X.; Wu, H.; Wang, J.; Lou, L.; Yin, K.; Gong, Y.; Shi, J.; Luo, Y.; Li, D.; et al. Control of the phase evolution of kesterite by tuning of the selenium partial pressure for solar cells with 13.8% certified efficiency. *Nat. Energy* **2023**, *8*, 526–535. [CrossRef]
10. Wada, T. Materials science of chalcopyrite-type and multinary solar cells compounds: Crystal structure and electronic structure of CISe, CZTS, CTS, and the related compounds. *JSAP Rev.* **2022**, *2022*, 220204. [CrossRef]
11. Meillaud, F.; Shah, A.; Droz, C.; Vallat-Sauvain, E.; Miazza, C. Efficiency limits for single-junction and tandem solar cells. *Sol. Energy Mater. Sol. Cells* **2006**, *90*, 2952–2959. [CrossRef]
12. Shockley, W.; Queisser, H.J. Detailed balance limit of efficiency of p-n junction solar cells. *J. Appl. Phys.* **1961**, *32*, 510–519. [CrossRef]
13. Rühle, S. Tabulated values of the Shockley-Queisser limit for single junction solar cells. *Sol. Energy* **2016**, *130*, 139–147. [CrossRef]
14. Ehrler, B.; Alarcón-Lladó, E.; Tabernig, S.W.; Veeken, T.; Garnett, E.C.; Polman, A. Photovoltaics reaching for the Shockley-Queisser limit. *ACS Energy Lett.* **2020**, *5*, 3029–3033. [CrossRef]
15. Yang, C.; Xue, R.P.; Li, X.; Zhang, X.Q.; Wu, Z.Y. Power performance of solar energy harvesting system under typical indoor light sources. *Renew. Energy* **2020**, *161*, 836–845. [CrossRef]
16. Shcherbachenko, S.; Astakhov, O.; Liu, Z.; Kin, L.C.; Zahren, C.; Rau, U.; Kirchartz, T.; Merdzhanova, T. High-bandgap perovskites for efficient indoor light harvesting. *Adv. Energy Sustain. Res.* **2024**, *5*, 2400032. [CrossRef]
17. Mengounou Mengata, G.; Ngoffe Perabi, S.; Ndi, F.E.; Wiysahnyuy, Y.S. Characterization of solar photovoltaic modules powered by artificial light for use as a source for smart sensors. *Energy Rep.* **2022**, *8*, 12105–12116. [CrossRef]
18. Karade, V.C.; Lim, J.; Gour, K.S.; Jang, J.S.; Shin, S.J.; Kim, J.H.; Yang, B.S.; Choi, H.; Enkhbat, T.; Kim, J.; et al. Overcoming the limitations of low-bandgap $Cu_2ZnSn(S,Se)_4$ devices under indoor light conditions: From design to prototype IoT application. *J. Mater. Chem. A* **2022**, *10*, 23831–23842. [CrossRef]
19. Scharber, M.C. Efficiency of emerging photovoltaic devices under indoor conditions. *Sol. RRL* **2024**, *8*, 2300811. [CrossRef]
20. Green, M.A.; Dunlop, E.D.; Yoshita, M.; Kopidakis, N.; Bothe, K.; Siefer, G.; Hao, X. Solar cell efficiency tables (version 62). *Prog. Photovolt. Res. Appl.* **2023**, *31*, 651–663. [CrossRef]
21. Massiot, I.; Cattoni, A.; Collin, S. Progress and prospects for ultrathin solar cells. *Nat. Energy* **2020**, *5*, 959–972. [CrossRef]
22. Polyanskiy, M.N. Refractive Index Database. Available online: https://refractiveindex.info (accessed on 17 February 2024).
23. Sai, H.; Umishio, H.; Matsui, T.; Nunomura, S.; Kawatsu, T.; Takato, H.; Matsubara, K. Impact of silicon wafer thickness on photovoltaic performance of crystalline silicon heterojunction solar cells. *Jpn. J. Appl. Phys.* **2018**, *57*, 08RB10. [CrossRef]
24. Scarpulla, M.A.; McCandless, B.; Phillips, A.B.; Yan, Y.; Heben, M.J.; Wolden, C.; Xiong, G.; Metzger, W.K.; Mao, D.; Krasikov, D.; et al. CdTe-based thin film photovoltaics: Recent advances, current challenges and future prospects. *Sol. Energy Mater. Sol. Cells* **2023**, *255*, 112289. [CrossRef]
25. Salhi, B. The photovoltaic cell based on CIGS: Principles and technologies. *Materials* **2022**, *15*, 1908. [CrossRef] [PubMed]
26. Earth Observation Group National Oceanic and Atmospheric Administration-Laboratory Spectra. Available online: https://ngdc.noaa.gov/eog/night_sat/spectra.html (accessed on 19 June 2023).
27. Elvidge, C.D.; Keith, D.M.; Tuttle, B.T.; Baugh, K.E. Spectral identification of lighting type and character. *Sensors* **2010**, *10*, 3961–3988. [CrossRef] [PubMed]

28. Minnaert, B.; Veelaert, P. A proposal for typical artificial light sources for the characterization of indoor photovoltaic applications. *Energies* **2014**, *7*, 1500–1516. [CrossRef]
29. Saha, A.; Haque, K.A.; Baten, M.Z. Performance evaluation of single-junction indoor photovoltaic devices for different absorber bandgaps under spectrally varying white Light-Emitting Diodes. *IEEE J. Photovolt.* **2020**, *10*, 539–545. [CrossRef]
30. Brendel, R.; Werner, J.H.; Queisser, H.J. Thermodynamic efficiency limits for semiconductor solar cells with carrier multiplication. *Sol. Energy Mater. Sol. Cells* **1996**, *41–42*, 419–425. [CrossRef]
31. Bronzoni, M.; Colace, L.; De Iacovo, A.; Laudani, A.; Lozito, G.M.; Lucaferri, V.; Radicioni, M.; Rampino, S. Equivalent circuit model for Cu(In,Ga)Se_2 solar cells operating at different temperatures and irradiance. *Electronics* **2018**, *7*, 324. [CrossRef]
32. Ho, J.K.W.; Yin, H.; So, S.K. From 33% to 57%-An elevated potential of efficiency limit for indoor photovoltaics. *J. Mater. Chem. A* **2020**, *8*, 1717–1723. [CrossRef]
33. Mahran, A.M.; Ganoub, M.; Kirah, K.; Abdellatif, S.O. Perovskite indoor light harvesters: From atomistic DFT to optoelectronic device modeling. *Optoelectron. Instrum. Data Process.* **2023**, *59*, 156–165. [CrossRef]
34. Mularso, K.T.; Jeong, J.-Y.; Han, G.S.; Jung, H.S. Recent strategies for high-performing indoor perovskite photovoltaics. *Nanomaterials* **2023**, *13*, 259. [CrossRef] [PubMed]
35. Feng, S.; Cheng, Y.; Yip, H.; Zhong, Y.; Fong, P.W.K.; Li, G.; Ng, A.; Chen, C.; Castriotta, L.A.; Matteocci, F.; et al. Roadmap on commercialization of metal halide perovskite photovoltaics. *J. Phys. Mater.* **2023**, *6*, 32501. [CrossRef]
36. Mathews, I.; Kantareddy, S.N.R.; Liu, Z.; Munshi, A.; Barth, K.; Sampath, W.; Buonassisi, T.; Peters, I.M. Analysis of CdTe photovoltaic cells for ambient light energy harvesting. *J. Phys. D Appl. Phys.* **2020**, *53*, 405501. [CrossRef]